

Hyper-Raman scattering analysis of the vibrations in vitreous boron oxide

G. Simon, B. Hehlen, R. Vacher, and E. Courtens
*Laboratoire des Colloïdes, Verres et Nanomatériaux (LCVN),
 UMR 5587 CNRS, University of Montpellier II, F-34095 Montpellier, France*
 (Dated: February 2, 2008)

Hyper-Raman scattering has been measured on vitreous boron oxide, $v\text{-B}_2\text{O}_3$. This spectroscopy, complemented with Raman scattering and infrared absorption, reveals the full set of vibrations that can be observed with light. A mode analysis is performed based on the local D_{3h} symmetry of BO_3 triangles and B_3O_3 boroxol rings. The results show that in $v\text{-B}_2\text{O}_3$ the main spectral components can be successfully assigned using this relatively simple model. In particular, it can be shown that the hyper-Raman boson peak arises from external modes that correspond mainly to librational motions of rigid boroxol rings.

PACS numbers: 63.50.+x, 78.30.Ly, 78.35.+c, 42.65.An

I. INTRODUCTION

Group theory provides a complete classification of the vibrational bands of crystals on the basis of symmetry. This, together with appropriate lattice dynamical calculations or simulations, generally allows relating the observed vibrational frequencies to specific atomic motions¹. Owing to structural disorder, such assignments are considerably more difficult in glasses. The structure of glasses at distances beyond the second atomic neighbours is hard to unravel using standard structural tools. However, the structural analysis generally reveals the existence of elementary structural units (ESUs) that are often similar to those in the corresponding crystals. The random network model² posits that these ESUs are connected to each other by looser bonds, with a broad distribution of interatomic distances and angles. Connected ESUs can also form larger structural groups that may not exist in the crystal. One example is given by ring structures, found for example in vitreous silica $v\text{-SiO}_2$, whose vibrations are observed in Raman scattering (RS).³ It is remarkable that vibrational spectroscopies of glasses mostly reveal well defined modes, pointing to specific vibrations of ESUs or groups of them. Structural information can be complemented by the analysis of these vibrations, and there have been frequent undertakings in that direction. Thus, the random network description provides a starting point for the analysis of vibrations.

In assigning the vibrations of glasses, a difficulty is that selection rules can be relaxed by either the distortion of the ESUs or by their environment. This is particularly severe for mixed covalent-ionic glasses. However, in purely covalent systems it can already be unsafe to assign modes based on RS or infrared (IR) absorption spectroscopies alone. For example, it often happens that modes observed in glasses with RS should in fact be inactive on the basis of the simple ESU symmetry. For this reason, it can be very useful to have results from an additional optical spectroscopy, namely hyper-Raman scattering (HRS). For example, the rigid librations of SiO_4 tetrahedra relating to the low frequency boson peak⁴ in $v\text{-SiO}_2$ should

be inactive in RS but they have been well identified in HRS^{5,6}. HRS also provides a useful complement to the more usual IR absorption spectroscopy. IR reflections can be sensitive to the state of the surface⁷, which is hard to control, while HRS probes the bulk. Also, the details of the spectral shapes of polar modes derived from IR reflectivity measurements can be blurred by the necessary Kramers-Kronig transformation. An example of that is shown below. It turns out that IR active modes can always be directly observed in HRS, with very specific selection rules⁸. As shown in this work, HRS spectroscopy is very helpful for the assignment of the vibrational modes of vitreous boron oxide, $v\text{-B}_2\text{O}_3$.

Boron oxide is an almost ideal glass former which hardly crystallizes at all. A specificity of $v\text{-B}_2\text{O}_3$ is that it contains *two* types of ESUs, the triangles BO_3 and the boroxol rings, B_3O_3 , while the single crystal at ambient pressure, which is rhombohedral with $Z=3$,⁹ contains *no* boroxol rings. For this reason, observing vibrations in the crystal would be of very limited guidance to assign the vibrations in the glass. The existence of boroxol rings in the glass is known from x-ray diffraction¹⁰, NMR¹¹, RS¹², and neutron scattering¹³. Although boroxols result from the bonding of three BO_3 triangles, these ESUs are special in that their internal B–O–B angle is $\cong 120^\circ$, while it is significantly larger for O atoms not belonging to boroxols as discussed below. The specific vibrations of boroxols have been the subject of several studies¹⁴. However, there has been a very long debate regarding the relative abundance of these rings which could not be ascertained from structure factors alone. It is only recently, with the help of NMR spectroscopy¹⁵ and of simulations of the vibrational spectra¹⁶ that it was established that approximately 3 out of 4 boron atoms belong to B_3O_3 rings in $v\text{-B}_2\text{O}_3$, although this result was further challenged^{17,18}.

In this paper we report the complete spectroscopy of $v\text{-B}_2\text{O}_3$ performed with both hyper-Raman scattering (HRS) and RS. HRS is a non-linear optical spectroscopy in which two incident photons of angular frequency ω combine with one excitation of the material at ω_v to produce one scattered photon at $2\omega \pm \omega_v$.⁸ The lower sign

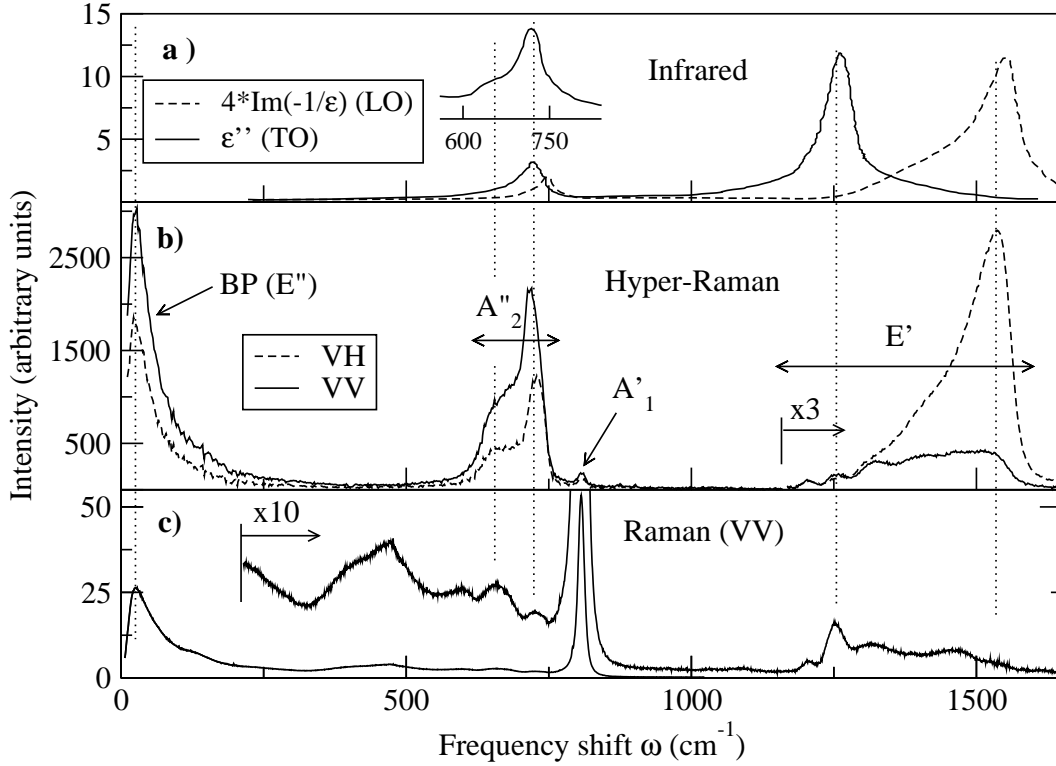


FIG. 1: Spectroscopy of $v\text{-B}_2\text{O}_3$: **a)** IR absorption from TO (—) and LO (---) derived from IR reflectivity measurements¹². The inset shows the lowest frequency polar band measured in transmission¹⁹ which is more structured than the TO peak derived from reflection; **b)** VV and VH hyper-Raman spectra obtained in 90° scattering; **c)** Raman (VV) spectrum from the same sample as in b). The frequencies are expressed in wavenumbers, $\omega/2\pi c$.

corresponds to a Stokes event (creation of a material excitation), while the upper sign is for an anti-Stokes event. RS was performed on the same sample in order to have fully comparable data. One interest in combining HRS with RS is that the selection rules of these two spectroscopies are often complementary, modes forbidden in RS being mostly allowed in HRS, and vice versa. Both longitudinal optic (LO) and transverse optic (TO) modes are active in HRS, with selection rules that allow separating them⁸. The results presented below will be compared to IR data from the literature. One can then identify clearly the TO and LO contributions. Spectra of pure $v\text{-B}_2\text{O}_3$ obtained in IR, RS, and HRS are presented in Fig. 1. The RS and HRS spectra are remarkably dissimilar. The polarized (VV) and depolarized (VH) HRS spectra exhibit three main bands plus a weak line around 808 cm^{-1} . The three intense bands are the boson peak (BP) at low frequencies, and TO-LO responses centered around 700 cm^{-1} and 1400 cm^{-1} . The latter are immediately identified as polar vibrations since they are strongly active in IR. The weakest HRS line around 808 cm^{-1} is the vibration that dominates the polarized RS spectrum. The BP, below $\sim 200\text{ cm}^{-1}$, is the only strong feature observed both in RS and in HRS.

The paper is organized as follows: in Section II, the experimental aspects are described, including the spectrom-

eter and the characterization of the sample; the structural model used for the description of the data is described in Section III; the analysis of the IR, RS, and HRS spectra is performed in sections IV, V, and VI, for the non-polar, polar, and boson-peak modes, respectively; finally, a discussion concludes the paper in Section VII.

II. EXPERIMENTAL ASPECTS

The HRS efficiency is usually very small, about 10^6 times weaker than the RS one. This explains that this spectroscopy was essentially restricted in the past to favorable nonlinear solids, such as ferroelectric oxides. Several recent instrumental advances, such as high power pulsed lasers, multichannel photo-counting devices, and large aperture and aberration corrected optical design, opened up the possibility for many new HRS investigations, particularly in glasses. In our setup, the hyper-Raman spectrum is excited by a diode pumped Q-switched YAG-laser emitting at the wavelength $\lambda = 1064\text{ nm}$.²⁰ For the experiments in B_2O_3 , we used typical repetition rates of 2500 Hz , leading to $\sim 20\text{ ns}$ pulse width. As this glass is very robust and optically transparent at this wavelength, it was possible to perform measurements with incoming peak powers up to $\sim 35\text{ kW}$

without alteration of the sample. The beam is focused with a $f=5$ cm lens to a ~ 20 μm diameter waist. The scattered light is collected by a $f/1.5$ photo-objective either in near forward-, in 90° -, or in back-scattering geometry. The polarization of the incident light is vertical (V), *i.e.* perpendicular to the scattering plane. That of the scattered light can be selected either V or H (horizontal) with an analyser that combines a half-wave plate with a wide band and large aperture Glan polarizer. The latter is fixed at V and the choice of the polarization V or H is done by 45° -rotation of the $\lambda/2$ -plate. Particular attention was given to accurate polarization measurements. To this effect, the setup was calibrated with the strongly polarized Raman line of CCl_4 at ≈ 460 cm^{-1} .²¹ This allowed estimating that the polarization leakage of our setup is below 0.1 %, at least up to that frequency range. The HRS spectra are dispersed with a Jobin-Yvon FHR-640 single-grating diffractometer of $f/5.6$ aperture, and detected with a nitrogen cooled CCD camera²². The dispersion of 2.4 nm/mm of the 600 grooves/mm grating allows covering a spectral range of $\simeq 2500$ cm^{-1} on the detector. This generally contains the full HRS spectrum. It is then acquired with a resolution of ~ 6 cm^{-1} (FWHM) using an entrance slit of 100 μm . A second grating with 1800 grooves/mm is also available for high resolution experiments. It zooms on a spectral range of about 800 cm^{-1} , with a spectral resolution of ~ 2 cm^{-1} (FWHM) at a 100 μm entrance slit. RS spectra of the same B_2O_3 sample were obtained with 514.5 nm excitation and analysed with a Jobin-Yvon T64000 triple-grating monochromator. We remark in passing that an attractive property of HRS in glasses, as compared to RS, is the inelastic over elastic signal ratio which is orders of magnitude more favorable in HRS, about 10^8 times larger. This provides a much better contrast at low frequencies, in particular in the BP region. In the high resolution single-grating mode, the tail of the hyper-Rayleigh line is generally negligible above 10 cm^{-1} , while RS would be very polluted by the elastic line in such a configuration.

The $v\text{-B}_2\text{O}_3$ sample was prepared from isotopically pure (99.6%) $^{11}\text{B}_2\text{O}_3$ containing ~ 1 wt% moisture. The material was heated to 1100 $^\circ\text{C}$ in a platinum crucible, quenched on a heat conducting plate, and annealed at 571 $^\circ\text{C}$ for 200 hours. Its water content, ~ 0.8 wt%, was measured by infrared transmission of a thin slice.²³ When required, $v\text{-B}_2\text{O}_3$ data were complemented by HRS from two lithium borate glasses, $4\text{B}_2\text{O}_3\cdot\text{Li}_2\text{O}$ and $2\text{B}_2\text{O}_3\cdot\text{Li}_2\text{O}$, kindly provided by Dr. A. Matic from Chalmers University of Technology, Göteborg, Sweden.

III. THE STRUCTURAL MODEL

The structure of vitreous boron oxide consists of a network of quasi-planar BO_3 triangles connected by their apical oxygens. Three triangles can associate to form a planar boroxol ring B_3O_3 . These two elementary structural units (ESUs), lone triangles and boroxol rings,

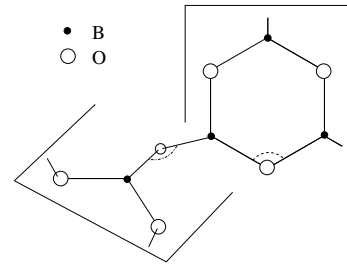


FIG. 2: Schematic assembly of a ring and a triangle in $v\text{-B}_2\text{O}_3$. These two ESUs form two B_2O_3 molecules. The relative orientation of the planes containing the triangle and the ring is random. It is the repetition of such patterns that produces the disordered network of $v\text{-B}_2\text{O}_3$ in this model. The possibility that occasionally two boroxols be directly connected with one $-\text{O}-$ atom, as in Fig. 11c below, is not excluded. However in that case there should also be two directly connected triangles, $-\text{B}_2\text{O}_5-$, for compensation.

are well defined, as seen from neutron diffraction¹³ and simulations¹⁶ results. The angular distribution of the O-B-O bonds is $120^\circ \pm 3.3^\circ$ in triangles,¹⁶ showing that they are rather flat. The boroxols are even closer to the perfect symmetry, as shown in Ref.¹⁶. The angular distribution of the B-O-B bonds bridging two ESUs is $\sim 130^\circ$ from Ref.^{10,24} or $134.4^\circ \pm 9.2^\circ$ from Ref.¹⁶. These have a much larger spread and they are also not restrained to the ESU plane, leading to the three dimensional random structure of the glass.

The spectra will be indexed according to a simple model in which only two types of ESUs are considered, the B_3O_3 boroxol rings and the BO_3 triangles (Fig. 2). Since the sum of one ring plus one triangle gives exactly two formula units, $2(\text{B}_2\text{O}_3)$, our model should contain the required number of modes if the glass would be composed exclusively of triangles and rings in the ratio 1:1. Alternatively, one could define the units as $\text{BO}_{3/2}$ and $\text{B}_3\text{O}_3\text{O}_{3/2}$, in the spirit of the split atom model²⁵. This has the merit to show that the ESUs transform as the equilateral triangles formed by the three $\text{O}_{1/2}$ splits atoms. However, this would be inconvenient for realistic calculations of the internal ESU vibrations, and it will not be adopted here. Our structural description is certainly very simplified. Strictly speaking, it only allows each triangle or ring to connect with three rings or triangles, respectively, while the real glass could contain interpenetrating ring networks, $m(\text{B}_3\text{O}_3 + -\text{O}-)$, and triangle networks, $\text{B}_n\text{O}_{2n+1}$. If less than 75% of boron atoms belong to rings, the glass will necessarily form other ESUs that preserve the stoichiometry, such as B_2O_5 , B_3O_7 , etc. Considering the dynamical properties, our model should nicely reproduce the vibrations of rings. However, it completely omits the $-\text{O}-$ bonds between two connected rings, and it can only partly index the $\text{B}_n\text{O}_{2n+1}$ motions in terms of vibration of BO_3 units.

TABLE I: Selection rules of modes in the point group D_{3h} , with the matrix elements for the Raman tensors¹, α_{ij}^ζ , and the symmetric hyperpolarisability tensors⁸, β_{ijk}^ζ . The latter are shown in the contracted indices notation.²⁶ The last column displays the eigenvectors of the normal modes for the flat CO_3 radical of calcite¹. T and R designate the 3 external translations and rotations respectively, the so-called non-genuine normal vibrations for isolated molecules.²⁷

Mode	IR	RS ¹	HRS ⁸	Normal modes ^{1,27}
A'_1		$\begin{vmatrix} a & \cdot & \cdot \\ \cdot & a & \cdot \\ \cdot & \cdot & b \end{vmatrix}$	$\begin{vmatrix} c & -c & \cdot & \cdot & \cdot & \cdot \\ \cdot & \cdot & \cdot & \cdot & \cdot & -c \\ \cdot & \cdot & \cdot & \cdot & \cdot & \cdot \end{vmatrix}$	
E'	(μ_x, μ_y)	$\begin{vmatrix} d & \cdot & \cdot \\ \cdot & -d & \cdot \\ \cdot & \cdot & \cdot \end{vmatrix}$ $\begin{vmatrix} \cdot & -d & \cdot \\ -d & \cdot & \cdot \\ \cdot & \cdot & \cdot \end{vmatrix}$	$\begin{vmatrix} 3e & e & f & \cdot & \cdot & \cdot \\ \cdot & \cdot & \cdot & \cdot & \cdot & e \\ \cdot & \cdot & \cdot & \cdot & f & \cdot \end{vmatrix}$ $\begin{vmatrix} \cdot & \cdot & \cdot & \cdot & e \\ e & 3e & f & \cdot & \cdot \\ \cdot & \cdot & f & \cdot & \cdot \end{vmatrix}$	
A''_2	μ_z		$\begin{vmatrix} \cdot & \cdot & \cdot & b & \cdot \\ \cdot & \cdot & b & \cdot & b \\ b & b & a & \cdot & \cdot \end{vmatrix}$	
A'_2			$\begin{vmatrix} \cdot & \cdot & \cdot & \cdot & -d \\ -d & d & \cdot & \cdot & \cdot \\ \cdot & \cdot & \cdot & \cdot & \cdot \end{vmatrix}$	R_z
E''		$\begin{vmatrix} \cdot & \cdot & \cdot \\ \cdot & \cdot & c \\ \cdot & c & \cdot \end{vmatrix}$ $\begin{vmatrix} \cdot & \cdot & -c \\ \cdot & \cdot & \cdot \\ -c & \cdot & \cdot \end{vmatrix}$	$\begin{vmatrix} \cdot & \cdot & \cdot & b & \cdot & \cdot \\ \cdot & \cdot & \cdot & \cdot & b & \cdot \\ \cdot & \cdot & \cdot & \cdot & \cdot & b \end{vmatrix}$ $\begin{vmatrix} \cdot & \cdot & \cdot & \cdot & -b & \cdot \\ \cdot & \cdot & \cdot & b & \cdot & \cdot \\ -b & b & \cdot & \cdot & \cdot & \cdot \end{vmatrix}$	R_x R_y

Regarding the symmetry properties, both BO_3 triangles and B_3O_3 boroxol rings belong to the point group D_{3h} . Hence, the vibrations decompose into the following irreducible representations :

$$[1, 2] A'_1 + [1, 2] A'_2 + [2, 2] A''_2 + [3, 4] E' + [1, 2] E'' \quad (1)$$

The figures within square brackets show the number of independent representations for triangles and rings, respectively. The IR, RS and HRS activities of each type of modes are summarized in Table I. These selection rules, derived for perfect symmetry,²⁸ do not account for possible distortions of the ESUs. In spite of the above mentioned limitations, we show in the following that the selection rules in Table I match remarkably well the experimental observations, thus allowing for a quantitative description of most vibrations of $v\text{-B}_2\text{O}_3$.

It is useful to provide a brief phenomenological description of the interaction of the ESUs with light. Light-scattering spectra are given by the Fourier transform of the space and time correlation functions of the dipole-moment fluctuations $\delta \mathbf{p}$ associated with vibrations and

induced in the material by an incident electric field $\mathbf{E} \propto e^{-i\omega_i t}$. For a structural unit m , the induced dipole \mathbf{p}^m can be expressed in terms of the local field \mathbf{E}^l as

$$\mathbf{p}^m = \chi_m^{(1)} \cdot \mathbf{E}^l + \frac{1}{2} \chi_m^{(2)} : \mathbf{E}^l \mathbf{E}^l + \dots \quad (2)$$

where $\chi_m^{(1)}$ and $\chi_m^{(2)}$ are the first and second-order polarizability tensors, respectively. Proper consideration of the local field is important for quantitative evaluations^{29,30}. However, for what symmetries are concerned, we assume that \mathbf{E}^l is essentially proportional to \mathbf{E} in a glass. It is the modulation of the polarizabilities by the normal modes of amplitude $W^\zeta \propto e^{\mp i\omega_\zeta t}$ for mode ζ , which leads to a modulation of \mathbf{p}^m at the Raman and hyper-Raman frequencies. One thus defines the molecular Raman and hyper-Raman polarizability-derivative tensors, $\alpha^{\zeta,m} = (\partial \chi_m^{(1)} / \partial W^\zeta)$ and $\beta^{\zeta,m} = (\partial \chi_m^{(2)} / \partial W^\zeta)$, respectively. In addition, if the dipole moment \mathbf{M}^m of the ESU m is modulated by the mode ζ , there is infrared absorption at ω_ζ , with an amplitude proportional to $\mu^{\zeta,m} = (\partial \mathbf{M}^m / \partial W^\zeta)$. The properties of the tensors $\mu^{\zeta,m}$, $\alpha^{\zeta,m}$, and $\beta^{\zeta,m}$, have been tabulated for all molec-

ular symmetries, *e.g.* in Ref.²⁸. Table I reproduces the results for the D_{3h} point group. In the Table, the orthogonal frame (x, y, z) is fixed to the ESU, with z perpendicular to the ESU plane, and x joining the center of the triangle to one of its vertices. The tensors in that frame will be written α^ζ and β^ζ . The vibrational eigenvectors for a AX_3 planar molecule are sketched in the last column of Table I.

As the two incident photons are at the same laser frequency ω_i , the hyper-Raman polarization fluctuation, $\delta \mathbf{p}^{\zeta, m} = \beta^{\zeta, m} : \mathbf{E}' \mathbf{E}^l W^\zeta$ leads to a scattered field at frequency $\omega_s = 2\omega_i \pm \omega_\zeta$. In this case the tensor β is obviously symmetric with respect to its last two indices, $\beta_{ijk} = \beta_{ikj}$. Moreover, since both ω_i and ω_s are far from any material resonance, β^ζ can be approximated as fully symmetric in all permutations of its three cartesian indices⁸. The corresponding scattering vector \mathbf{q} is given by $\mathbf{q} = \pm(\mathbf{k}_s - 2\mathbf{k}_i)$, where \mathbf{k}_s and \mathbf{k}_i are the wave vectors of the scattered and incident radiation, respectively.

The integrated HRS intensity for mode ζ , projected onto a unit polarization vector \mathbf{e} , is proportional to the square of the corresponding polarization density. The latter is given by a sum over the m ESUs vibrating at W^ζ within a unit volume,

$$I_{\text{HR}}^\zeta \propto \left| \sum_m \mathbf{e} \cdot \delta \mathbf{p}^{\zeta, m} \right|^2. \quad (3)$$

In the case of B_2O_3 , our model implies that the sum extends only over triangles, or only over rings, depending on the particular mode ζ .

IV. HYPER-RAMAN SCATTERING FROM NON-POLAR MODES

When each ESU vibrates independently from the others, the cross terms in Eq. 3 vanish on the average, and the summation can be extracted from the square. Similarly to the Raman case, one obtains then for the *incoherent* hyper-Raman scattering intensity,

$$I_{\text{HRS}}^{\zeta, \text{inc}} \propto \sum_m \left| \mathbf{e} \cdot \beta^{\zeta, m} : \mathbf{E} \mathbf{E} \right|^2. \quad (4)$$

Eq. (4) generally applies to non-polar *internal* vibrations. The scattering is then “local” and thus independent of \mathbf{q} . Implicit in Eq. (4) is the fact that the polarization vectors are fixed in the laboratory frame, while in a glass different ESUs have different orientations in that frame. Hence, Eq. (4) implies an angular averaging. The explicit calculation of (4) involves three rotation matrices in each term, to bring β^ζ from the table to the particular $\beta^{\zeta, m}$ for each ESU m , or conversely and more conveniently, to rotate \mathbf{E} and \mathbf{e} to the ESU frame. For a macroscopically isotropic medium this averaging is uniform, leading to results which are found *e.g.* in Ref.³¹. One defines a depolarization ratio for mode ζ ,

$$\rho_{\text{HRS}}^{\zeta, \text{inc}} = I_{\text{VH}}^{\zeta, \text{inc}} / I_{\text{VV}}^{\zeta, \text{inc}}, \quad (5)$$

where VV stands for $\mathbf{e} \parallel \mathbf{E}$, while VH means $\mathbf{e} \perp \mathbf{E}$. For the local D_{3h} symmetry of B_2O_3 , one has $\rho_{\text{HRS}}^{\zeta, \text{inc}} = 2/3$ for all non-polar modes³¹, a result which will be important in the mode analysis below, as it allows distinguishing polar excitations from incoherent contributions.

There is at least one feature in the HRS spectra that can be unambiguously associated with a non-polar vibration. It is the relatively weak line at 808 cm^{-1} on Fig. 1b which gives the narrow peak dominating the Raman spectrum (Fig. 1c). This mode was assigned long ago to radial breathing motions of boroxol rings³². The proposal that it might relate to a coherent symmetric stretch of the bridging oxygens over the entire network³³ should be abandoned in this particular case, since the large spread in -B-O-B- angles outside boroxol rings could not produce such a narrow width. Raman scattering from isotopically pure samples containing ^{10}B , ^{11}B , ^{16}O , and ^{18}O , has established beyond reasonable doubt that this mode is associated with a local symmetric stretch A'_1 within boroxols³². It is the remarkable regularity of the boroxols that accounts for the narrowness of this vibration. The eigenvectors, sketched in the inset of Fig. 3, are completely dominated by the oxygen motion, as confirmed by isotopic substitution³². Incidentally, this explains that this motion essentially does not couple different boroxol rings. The vibration is non-polar, and thus inactive in IR, as observed in Fig. 1. From Table I, it is also expected to give intensity both in RS and HRS which is indeed confirmed by the experiment. In fact, it is the same transition matrix elements that are involved in the microscopic calculation of α_{xx} and β_{xxx} .⁸ Therefore there is no reason to believe that the HRS activity should be anomalously small compared to the RS activity. Hence, the relative size of the A'_1 peaks observed in the two spectroscopies does provide a scale for the comparison of the spectral intensities. The relatively large strength of the other features observed in HRS must derive from the coherent enhancement of these signals³⁴, as explained below.

Figure 3 shows the detail of our Raman and hyper-Raman polarized (VV) and depolarized (VH) spectra. It is already known that the RS signal is strongly polarized for this particular mode. A depolarization ratio $\rho_{\text{RS}}^{A'_1} = I_{\text{VH}}/I_{\text{VV}} = 1/28$ was reported in Ref.¹². In our most reliable measurement shown in Fig. 3a, we find $\rho_{\text{RS}}^{A'_1} = 1/23$. All normal modes of D_{3h} symmetry have a RS depolarization ratio equal to $3/4$, except for A'_1 modes. The depolarization ratio of A'_1 is different as there is an additional contribution to I_{VH} arising from $\alpha_{xx} \neq \alpha_{zz}$. The inverse ratio is then given by

$$\frac{I_{\text{VV}}}{I_{\text{VH}}} = \frac{1}{\rho_{\text{RS}}^{A'_1}} = \frac{5}{3} \left(\frac{2\alpha_{xx} + \alpha_{zz}}{\alpha_{xx} - \alpha_{zz}} \right)^2 + \frac{4}{3},$$

leading to strongly polarized lines as soon as $\alpha_{xx} \simeq \alpha_{zz}$. For a depolarization ratio equal to $1/23$ there are two possibilities : either $\alpha_{xx} = 2.86\alpha_{zz}$ or $\alpha_{xx} = 0.46\alpha_{zz}$. With the covalent bonds in plane, the former seems more

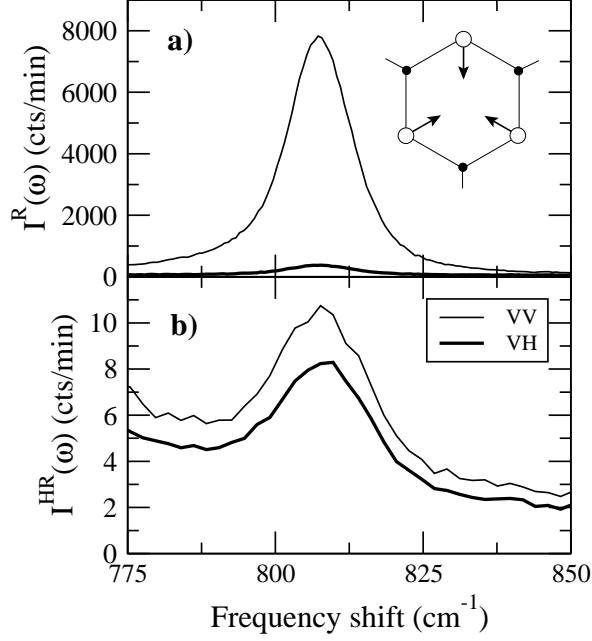


FIG. 3: Polarization measurement of the breathing mode of boroxol rings in v -B₂O₃ (A'_1 symmetry): **a)** RS, and **b)** HRS.

likely. In HRS we find $\rho_{HRS}^{A'_1} \simeq 0.67 \pm 0.015$ (Fig. 3b), in very good agreement with the theoretical value of $2/3$. Interestingly, we find that this mode perfectly fulfills the selection rules for incoherent scattering. This certainly arises from the very regular structure of the boroxol rings in the glass and from the fact that only the oxygen atoms move. It is now of interest to investigate whether the selection rules, which apply so well for $\zeta = A'_1$, are also satisfied for the other boroxol vibrations.

V. HYPER-RAMAN SCATTERING FROM POLAR MODES

In situations where several units vibrate with a fixed phase relationship, there is *coherence*, and the cross products in the development of Eq. 3 cannot be neglected. In HRS, this occurs in two important cases: (i) for *polar vibrations*, where the dipole-induced electric field imposes an extended phase relationship in the material, and (ii) for *external modes*, e.g. for librations in which adjacent units move together like cogwheels, also leading to a certain degree of coherence. The intensity in Eq. 3 can be separated into two terms,

$$I_{HR}^{\zeta} \propto \sum_m |\delta \mathbf{p}^{\zeta, m}|^2 + \sum_{m \neq n} \delta \mathbf{p}^{\zeta, m} \cdot \delta \mathbf{p}^{\zeta, n} \quad (6)$$

TABLE II: Selection rules for TO and LO modes in the average ($\infty\infty m$) symmetry group.

Scat. geometry	I_{VV}	I_{VH}	I_{HV}	I_{HH}
90°	$9a_{TO}^2$	$\frac{1}{2}a_{TO}^2 + \frac{1}{2}a_{LO}^2$	a_{TO}^2	$\frac{1}{2}a_{TO}^2 + \frac{1}{2}a_{LO}^2$
180°	$9a_{TO}^2$	a_{TO}^2	a_{TO}^2	$9a_{TO}^2$
$0^\circ + \text{vert. slit}$	$9a_{LO}^2$	a_{TO}^2	a_{LO}^2	$9a_{TO}^2$

A. Selection rules

The important point is that the scattered intensity for modes of type (i) or (ii) is affected by the coherent term on the right hand side of Eq. 6. For isotropic (*i.e.* incoherent) averaging, the sum over $\delta \mathbf{p}^{\zeta, m} \cdot \delta \mathbf{p}^{\zeta, n}$ in Eq. 6 is zero. It is the existence of correlations between the units m and n that gives weight to this term. For polar modes, the correlation function depends on the symmetry of the vibrations and on the polarization field. Its calculation is beyond the scope of this paper. A device to account for this anisotropic averaging is to separate β^ζ in two terms, $\beta^\zeta = \Delta\beta^\zeta + \bar{\beta}^\zeta$.³⁵ $\Delta\beta^\zeta$ corresponds to the local scattering process and has the symmetry specified in Section III, while $\bar{\beta}^\zeta$ corresponds to a modulation over the average $\infty\infty m$ glass symmetry. The properties of the latter are condensed into a single matrix³⁵:

$$\bar{\beta}^\zeta = \begin{vmatrix} XX & YY & ZZ \\ 3a^\zeta & a^\zeta & a^\zeta \\ a^\zeta & 3a^\zeta & a^\zeta \\ a^\zeta & a^\zeta & 3a^\zeta \end{vmatrix} \begin{matrix} X \\ Y \\ Z \end{matrix} \quad (7)$$

where X , Y , and Z are laboratory-fixed axes. Similarly to Table I, the double and single indices correspond to the two incident photons and to the scattered photon, respectively. The value of a^ζ depends on the mode ζ and it is different for TO and LO. In the extreme case, where $\bar{\beta}^\zeta$ fully dominates the scattering, one should observe a constant depolarization ratio $\rho_{coh} = (\bar{\beta}_{HV}^\zeta / \bar{\beta}_{VV}^\zeta)^2 = 1/9$.

Finally, the scattered intensity of these collective waves also depends on the wave vector \mathbf{q} , as shown on Fig. 4. The selection rules depend on the scattering geometry. From these pictures, and the tensor elements (7), one easily calculates the expected intensities for the TO and LO modes in the perfect $\infty\infty m$ symmetry. These are summarized in Table II, where one sees that both TO and LO scatter at 90° , while only TO modes are active in backscattering. In near-forward scattering, the wave vector \mathbf{q} is perpendicular to the optical axis. It can take all orientations around this axis (Fig. 4c) and the scattering plane is undefined. To be able to define the polarization, it is necessary to restrict \mathbf{q} to a plane. This is achieved by a slit placed at the exit pupil of the collecting lens (Fig. 4c). A vertical slit defines a vertical scattering plane, while a horizontal slit gives a horizontal scattering plane. In our implementation, the slit reduces the internal angular aperture to $\sim 4^\circ$ perpendicular to its direction, leading to an almost complete removal of the

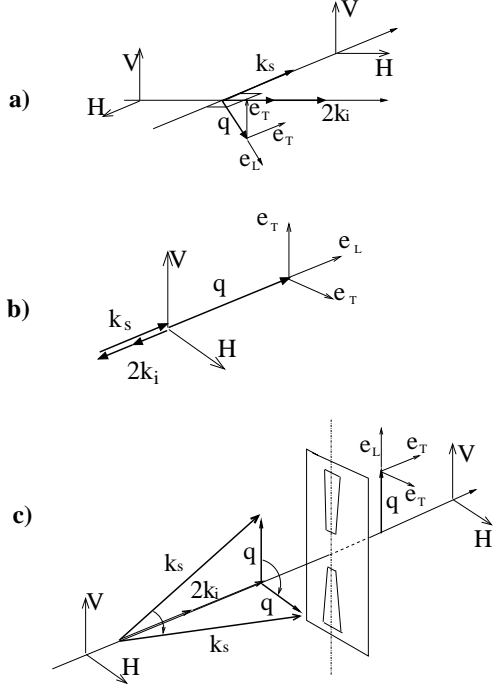


FIG. 4: HRS scattering geometries and polarization of the TO (e_T) and LO (e_L) components: **a)** 90°-scattering, **b)** backscattering, **c)** near-forward scattering. For the latter, the vertical diaphragm is used to select only the LOs in a VV spectrum.

TO contribution from VV spectra in the configurations of Fig. 4c. The reduction of the TO is estimated to be by a factor ~ 25 . This allows measuring the LO mode alone, with an intensity $I_{VV} \propto 9a_{LO}^2$. Alternatively, the TO alone is observed in HH polarization with an intensity proportional to $9a_{TO}^2$. This permits the measurement of the LO/TO intensity ratio.

Returning to B_2O_3 , there are two types of IR active modes in the D_{3h} point group: the polar vibrations of symmetry A_2'' and those of symmetry E' . The A_2'' modes correspond to out-of-plane motions. One eigenvector is a translation of the rigid ESUs which are charged (T_z), while the other is an internal vibration with displacements of the B and O atoms in opposite directions (see Table I). The E' modes are in-plane motions. One representation corresponds to translations of the rigid ESUs (T_x , T_y), while the others are internal vibrations, as shown for example in Table I. These two types of modes are associated with the broad bands centered at ~ 700 cm^{-1} and ~ 1400 cm^{-1} , respectively. These modes are naturally present in IR absorption (TO) and IR reflectivity (LO), as shown in Fig. 1. Small frequency differences in the positions of the main maxima observed in different spectroscopies could partly originate from differences in the samples. However, one cannot exclude an intrinsic property arising from the specificities of IR and HRS spectroscopies, which are sensitive to fluctuations of first

and third rank tensors, respectively⁸. In order to determine the symmetry of the modes on the basis of the analysis above, we performed 90°, 180°, and 0°-scattering spectroscopies of the A_2'' and E' polar bands of v - B_2O_3 .

B. Out-of-plane displacements A_2''

The restoring forces for out-of-plane displacements are significantly smaller than for in-plane ones. According to Ref.³⁶, the HRS band at ~ 700 cm^{-1} can thus be attributed to A_2'' modes. Fig. 5 shows separately the TO

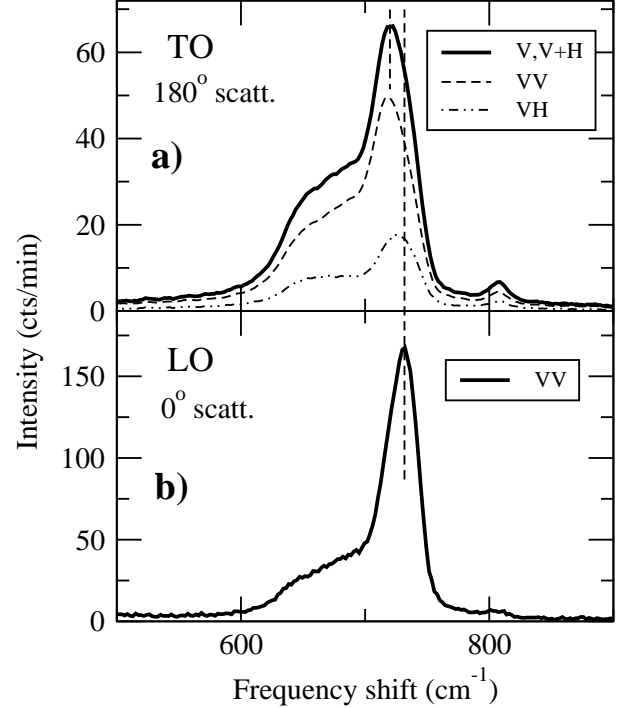


FIG. 5: Decomposition of the **a)** TO and **b)** LO responses for the A_2'' vibrations. The LO components (V,V) has been obtained in forward scattering with a *vertical* slit, as explained in the text.

and LO contributions for these modes. As only the TOs scatter in backscattering, it is straightforward to extract their depolarization ratio. We find $\rho_{exp}^{A_2''} = 0.36 \pm 0.01$ at 720 cm^{-1} , far from the value $1/9$ expected for scattering arising only from β . This type of discrepancy was observed in all the glasses that we investigated so far.³⁷ We believe it originates from the local term $\Delta\beta^c$ which also contributes to scattering. The depolarization ratio slightly depends on the frequency, as revealed by the different profiles of the VV and VH spectra in Fig. 5a. The TO clearly exhibits a double-peak structure with a broad component centered around 665 cm^{-1} and a more intense narrow one at 720 cm^{-1} . It is known from IR spectroscopy (see Fig. 1) that the LO mode is not far from the TO one. In that case, the LO can be measured alone by performing HRS in near forward scattering (Fig. 4c).

The doublet is also seen in this LO response presented in Fig. 5b. The maximum of the sharp LO component is at 731 cm^{-1} , which gives a small TO-LO splitting of only 11 cm^{-1} for this particular spectral component. A significant value for the TO-LO splitting cannot be extracted for the broad component.

To gain further information it is now interesting to compare $v\text{-B}_2\text{O}_3$ to the lithium borate glasses $4\text{B}_2\text{O}_3\text{:Li}_2\text{O}$ and $2\text{B}_2\text{O}_3\text{:Li}_2\text{O}$. A major effect of lithium in boron oxide is to produce BO_4 tetrahedra for charge compensation. This dramatically reduces the concentration of boroxol rings. The disappearance of the A'_1 breathing mode at 808 cm^{-1} in Fig. 6b is a clear signature for this. As the number of rings is reduced with increasing Li content, the two maxima in Fig. 6b transform into a single peak at an intermediate frequency of $\approx 696\text{ cm}^{-1}$. Hence, we associate the sharp line of B_2O_3 at $\approx 720\text{ cm}^{-1}$ to A''_2 vibrations of rings, and the broader contribution at 665 cm^{-1} to A''_2 vibrations of triangles. This trend has been recently confirmed by first principle calculations: making the rings silent in the simulation shifts the position of the A''_2 peak to lower frequencies³⁸. The eigenvectors of the A''_2 vibration for triangles and

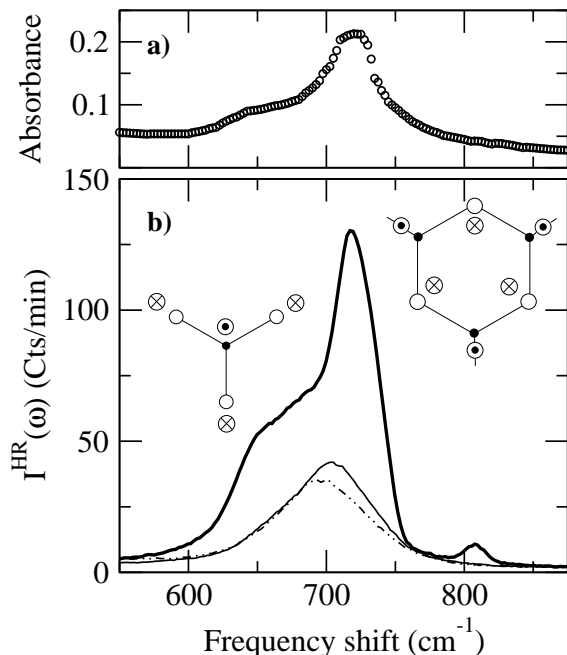


FIG. 6: **a)** A''_2 polar band in B_2O_3 as obtained from IR transmission¹⁹. **b)** HRS VV spectra from the A''_2 polar band in borate glasses obtained in 90° -scattering: “—” $v\text{-B}_2\text{O}_3$, “— — —” $4\text{B}_2\text{O}_3\text{:Li}_2\text{O}$, and “- · - · -” $2\text{B}_2\text{O}_3\text{:Li}_2\text{O}$.

rings are shown in Fig. 6b. Returning to Fig. 1, one notes that the A''_2 vibrations are also observed in RS, although they should be forbidden by symmetry for perfect ESUs (see Table I). However, this neglects center-of-mass motion which is Raman active. Also, a small departure

from perfect planarity induces a permanent dipole moment that very effectively relaxes the Raman selection rule. Thus, the RS signal could arise from vibrations of non-planar ESUs. The rings, being more regular than the triangles, should then give a weaker relative intensity in RS than in IR and HRS, which agrees with observations in Fig. 1c.

C. In-plane displacements E'

The weaker HRS efficiency, and the many components belonging to the band centered at $\sim 1400\text{ cm}^{-1}$, do not allow for such detailed quantitative analysis as done for the A''_2 band. In that case the LO is clearly separated from the TO (Fig. 1a) and not much would be gained by showing our measurement similar to that in Fig. 5b. Fig.

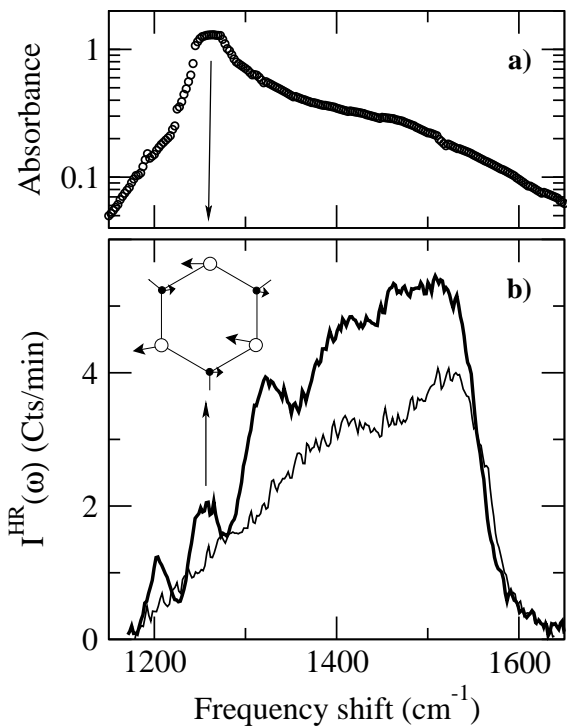


FIG. 7: **a)** E' polar modes of $v\text{-B}_2\text{O}_3$ as obtained from IR transmission¹⁹ on a semi-logarithmic scale. **b)** 90° -scattering hyper-Raman spectra (VV) from the E' polar modes of $v\text{-B}_2\text{O}_3$ (bold line) and $4\text{B}_2\text{O}_3\text{:Li}_2\text{O}$ (thin line).

7b zooms on the 1400 cm^{-1} frequency region in a geometry which does not scatter the LO. Unlike A''_2 modes, these high frequency vibrations exhibit a completely different shape in HRS and IR. The main IR line at 1265 cm^{-1} is found in HRS, but with a rather weak intensity. Its depolarization ratio is roughly estimated to be $\rho_{HR} = 0.37 \pm 0.05$, again far from $1/9$ but also smaller than the value $2/3$ that would apply to non-polar dis-

placements. This confirms that this mode is polar in nature. It is also expected to be active in RS (Table I), with a depolarization ratio of 3/4, which is observed in experiment. The activity of the line at 1265 cm^{-1} in IR, RS, and HRS suggests an internal polar vibration E' of the D_{3h} point group (Table 1). The mode disappears in the lithium borate glass $4B_2O_3:Li_2O$ (Fig. 6b), confirming³⁹ that it is associated with motions in rings. As it dominates the IR absorption spectra, it must correspond to displacements with the largest dipole moment fluctuations. From isotopic substitution, it was shown that this mode mainly involves the oxygen atoms³². This presumably also implies coupling with the center of mass motions (T_x , T_y). A tentative eigenvector is sketched in Fig. 7b.

In addition, the HRS spectra exhibit two narrow lines at 1210 cm^{-1} and 1325 cm^{-1} , plus two broad bands at higher frequencies, ~ 1400 and $\sim 1500\text{ cm}^{-1}$. The three peaks on the low frequency side clearly disappear in the lithium borate HRS spectrum of Fig. 7b. We conclude that the narrow lines are associated with motions in boroxols, and that the broad bands correspond to motions in triangles. This confirms previous RS assignments³⁹. Finally, the comparison between these two spectra possibly reveals another ring vibration around 1460 cm^{-1} . In any case, there seems to be sufficient richness in this band to fully account for the five E' internal vibrations listed in (1).

D. Polaritons in near-forward scattering

Polaritons originate from the electro-mechanical coupling between transverse polar modes and the incident electromagnetic field. This photon-phonon interaction requires that both the frequencies and wave vectors of both types of modes match, which occurs at small scattering angles $\sim \omega_{TO}/\omega_i$, *i.e.* in near-forward scattering. Owing to this interaction, the phase velocity of transverse polarization waves cannot exceed the speed of light in the medium. In consequence, for scattering angles decreasing typically below 10° , the frequency of the TO modes decreases down to the nearest LO component, with a slope smaller than that of the photon branch¹. The observation of polaritons by HRS was pioneered by Denisov *et al.*⁸. A detailed analysis of their properties in borate glasses is not the purpose of this paper. However, the observation of this coupling can be very helpful to determine the polar character of vibrations. The VV spectrum presented in Fig. 8 (thin line) has been obtained in near forward scattering with angles θ in the sample integrated from 4° to 20° , and a horizontal slit in order to reject the LO modes. A strong polariton is clearly visible around 1180 cm^{-1} . It is presumably associated with the main polar E' vibration at 1265 cm^{-1} . In contrast, the polariton associated with the polar A_2'' modes is very weak. It is shown by the arrow in the inset. For this scattering geometry the TOs are active with an intensity $I \propto 9a_{TO}^2$. The re-

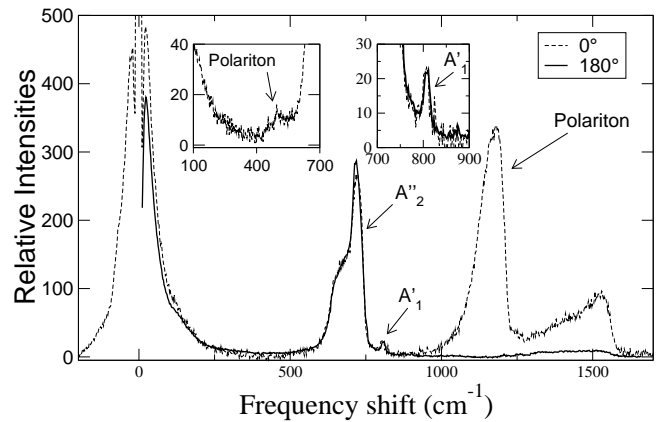


FIG. 8: Comparison between near-forward and backscattering HRS spectra with VV analysis. The former has been obtained using a *horizontal* slit in order to select only the TO polar components. The left inset zooms on the small polariton associated with the A_2'' TO band. The two spectra have been normalized in intensity to the maximum of the incoherent A_1' mode shown in the right inset.

sult is compared with the backscattering HRS response obtained in VV (bold line) which also measures only the TO modes with $9a_{TO}^2$. As an incoherent and non-polar scatterer, the intensity of the A_1' mode does not depend on the wave vector \mathbf{q} . Owing to this, it is possible to scale the spectra at 0° and 180° to the maximum of this mode. The observed differences should essentially arise from the polariton activity. This unambiguously shows that there exists polaritons in the entire broad band from ~ 1200 to $\sim 1600\text{ cm}^{-1}$. A detailed analysis of this complex band could presumably only be achieved with careful simulations.

Looking at the boson peak region, one observes an intensity excess in near-forward scattering. This would also deserve a more detailed analysis. This \mathbf{q} -dependence of the intensity suggests a small polar component in the BP. However, our data at 90° and 180° are very similar and the polarization analysis gives the same depolarization ratio $\rho = 0.60$ at the BP maximum for both scattering geometries,³⁷ while the LOs are active in 90° (VH) and silent in backscattering. We conclude from the above that there exist motions in the BP of B_2O_3 which induce fluctuations of the dipolar moment, but that the dominant modes in HRS from the BP are non-polar in nature.

VI. THE BOSON PEAK

The last main feature in HRS is the boson peak (BP) at low frequencies. Following our model, it is unlikely that the microscopic origin of the BP relates to any *internal* vibration of the D_{3h} point group as they have mostly been assigned in former Sections. However, there remains *external* vibrations, the translations (\mathbf{T}) and the rotations (\mathbf{R}) of rigid ESUs. These motions are non-genuine vi-

brations for isolated molecules.²⁷ They are characterized by diffusive relaxation in the liquid phase and transform into real vibrations, usually at low frequencies, in the glass phase. Hence, one should use the term “libration” to designate angular oscillations of the ESUs in the latter case, as the mean equilibrium orientations are then fixed. For what translations are concerned, they should not be confused with long wave acoustic modes. The latter are collective waves whose HRS is strictly forbidden in the $\infty\infty m$ symmetry of the glass phase.⁸ However quasi-local relative displacements of nearby ESUs can be active in HRS from glasses just as optic modes are in crystals.

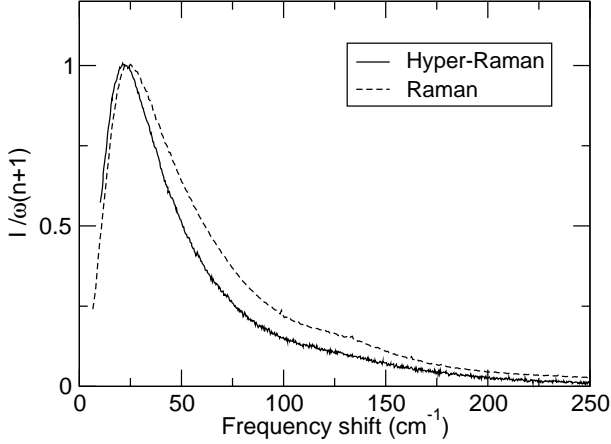


FIG. 9: VH spectra of the RS (---) and HRS (—) boson peaks. The data are normalized to the BP maximum.

Figure 9 shows that HRS and RS BPs, although not identical, are very similar. It suggests that the BP modes are active in both spectroscopies. It has been shown, using lithium borate glasses, *e.g.* in Ref.⁴⁰, that the RS BP of $v\text{-B}_2\text{O}_3$ is dominated by boroxol-ring motions rather than by triangle motions. The same applies to HRS as we observed a strong decrease in the intensity of the BP in lithium borate samples. This further supports the idea that the same modes contribute to the RS and HRS BPs. Proceeding by elimination, and taking into account that in-plane librations (A'_2) are hard motions silent in RS, the only remaining possibility for the BP is out-of-plane librations of rings (E'' modes) coupled to their relative translations. The translations are active in IR (Table I) and this could explain the excess signal on the BP that is observed in near-forward scattering (Fig. 8). However, it has been shown in liquids that the low frequency HRS signal is mainly dominated by the rotational component of the external motions rather than by translational ones^{41,42}. For example, liquid CCl_4 is composed of tetrahedra belonging to the point group T_d . The strong relaxational hyper-Rayleigh line of CCl_4 was analyzed as the sum of a narrow and a broad lorentzian. The narrow component was interpreted in terms of rotational diffusion and the broad one was attributed to *collective* intermolecular orientational motions⁴². It is intuitive that in network glasses, rigid translations or librations of one

ESU do couple with neighbouring ESU motions. Depending on the nature of the relative displacements of the structural units, this can lead to constructive or destructive coherent effects in scattering. If constructive

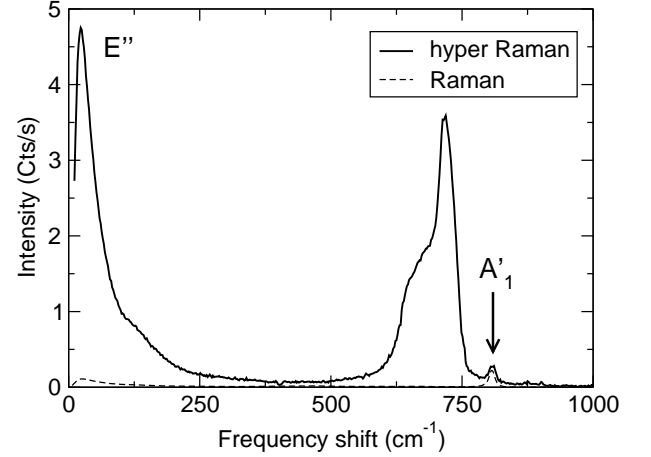


FIG. 10: Raman and hyper-Raman spectra of $v\text{-B}_2\text{O}_3$. The intensities are normalized to the area of the A'_1 mode active in both spectroscopies. This presentation emphasizes the comparatively strong efficiency of the BP in HRS.

coherence occurs, it can lead to an anomalously strong HRS efficiency, which is indeed observed as seen in Fig. 10. The intensity of the BP is comparable that of the strongest polar vibrations which are coherent scatterers in HRS. Incoherent non-polar vibrations give a relatively weak HRS signal, as shown by the A'_1 mode discussed in Section IV. The scattering efficiency of the BP relative to the breathing A'_1 -mode is much larger in HRS than in RS. This is emphasized by the normalization used for Fig. 10.

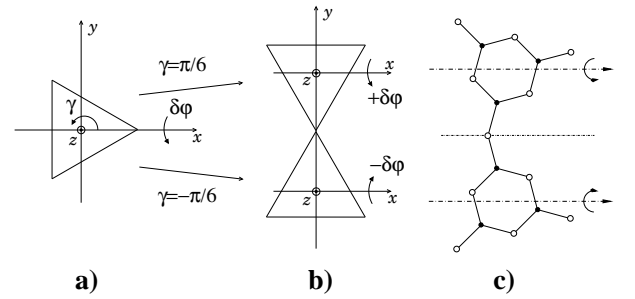


FIG. 11: Definition of the axes and rotation angles for a single ESU (a) and for a particular out-of-plane libration of two adjacent ESUs (b); (c) shows a possible ESU configuration approximating (b).

Coherent effects on the RS and HRS BP relate to the symmetries of the polarizability and hyper-polarizability tensors of the E'' modes. To show how this can occur, we present now a simple calculation for a particular coherent libration of a pair of ESUs. In the D_{3h} point group,

both BO_3 and B_3O_3 rings transform like equilateral triangles (Fig. 11). For the boroxols, the B atoms point to the apices of these triangles owing to their bonding to external O atoms. The Raman susceptibility $\chi^{(1)}$ can be decomposed into its isotropic and anisotropic parts. We neglect the modification of the isotropic tensor by librations, as this must be a second order effect. The traceless anisotropic part has elements $\chi_{11}^{(1)} = \chi_{22}^{(1)} = -\frac{1}{2}\chi_{33}^{(1)}$. For convenience we write $\chi_{11}^{(1)} \equiv -c/3$. Now consider that the ESU of Fig. 11a is rotated by a finite angle γ around the z -axis and that it librates by an angle $\delta\varphi$ around the initial x -axis. The in-plane rotation by γ does not modify $\chi^{(1)}$, while the out-of-plane libration around x modulates it by

$$\delta\chi_x^{(1)} = \delta\varphi \begin{vmatrix} \cdot & \cdot & \cdot \\ \cdot & \cdot & c \\ \cdot & c & \cdot \end{vmatrix}, \quad (8)$$

One should note that, similarly, a libration by $\delta\phi$ around the y -axis gives

$$\delta\chi_y^{(1)} = \delta\phi \begin{vmatrix} \cdot & \cdot & -c \\ \cdot & \cdot & \cdot \\ -c & \cdot & \cdot \end{vmatrix}. \quad (9)$$

One recognizes then in Eqs. (8) and (9) the two tensors transforming like R_x and R_y in the last entry of Table I.

Consider now the hyper-Raman second-order susceptibility tensor $\chi^{(2)}$. With the definition of axes in Fig. 11a, the only nonvanishing elements are $\chi_{111}^{(2)} = b = \chi_{11}^{(2)}$, $\chi_{122}^{(2)} = -b = \chi_{12}^{(2)}$, and $\chi_{221}^{(2)} = \chi_{212}^{(2)} = -b = \chi_{26}^{(2)}$, where contracted indices²⁶ are used in the last term of the equalities. The structure of that tensor is identical to that in the first entry of Table I. We call it $\chi_X^{(2)}$, indicating that an apex of the triangle lies on the positive x axis. Now, if the triangle is rotated by $\gamma = \pi/2$, so that an apex lies on the positive y -axis, one finds $\chi_{21}^{(2)} = \chi_{16}^{(2)} = b$ and $\chi_{22}^{(2)} = -b$. This is called $\chi_Y^{(2)}$, so that

$$\chi_X^{(2)} = \begin{vmatrix} b & -b & \cdot & \cdot & \cdot \\ \cdot & \cdot & \cdot & \cdot & -b \\ \cdot & \cdot & \cdot & \cdot & \cdot \end{vmatrix}, \quad \chi_Y^{(2)} = \begin{vmatrix} \cdot & \cdot & \cdot & \cdot & b \\ b & -b & \cdot & \cdot & \cdot \\ \cdot & \cdot & \cdot & \cdot & \cdot \end{vmatrix}. \quad (10)$$

Incidentally, the latter form corresponds to the choice of axes in Ref.⁴³. Now, if $\chi^{(2)}$ is rotated by an arbitrary angle γ , one simply finds

$$\chi_\gamma^{(2)} = \cos 3\gamma \chi_X^{(2)} + \sin 3\gamma \chi_Y^{(2)}. \quad (11)$$

Librating $\chi_X^{(2)}$ and $\chi_Y^{(2)}$ around the x -axis by $\delta\varphi$, one obtains

$$\delta\chi_{X,x}^{(2)} = \delta\varphi \begin{vmatrix} \cdot & \cdot & \cdot & b & \cdot & \cdot \\ \cdot & \cdot & \cdot & \cdot & b & \cdot \\ \cdot & \cdot & \cdot & \cdot & \cdot & b \end{vmatrix},$$

$$\delta\chi_{Y,x}^{(2)} = -\delta\varphi \begin{vmatrix} \cdot & \cdot & \cdot & -b & \cdot & \cdot \\ \cdot & \cdot & \cdot & b & \cdot & \cdot \\ -b & b & \cdot & \cdot & \cdot & \cdot \end{vmatrix}. \quad (12)$$

Again, one recognizes the tensors in the last row of Table I. For R_x the identity is immediate. For R_y it results from $\delta\chi_{X,y}^{(2)}/\delta\phi = -\delta\chi_{Y,x}^{(2)}/\delta\phi$, as R_y corresponds to the libration of $\chi_X^{(2)}$ around y . Finally, from (11), the fluctuating susceptibility for a libration around x of an ESU rotated by γ around z simply is

$$\delta\chi_{\gamma,x}^{(2)} = \cos 3\gamma \delta\chi_{X,x}^{(2)} + \sin 3\gamma \delta\chi_{Y,x}^{(2)}. \quad (13)$$

With the above, one can now calculate the RS and HRS responses of *two* ESUs connected by a common apex that moves perpendicularly to the plane of the drawing. Fig. 11b show the case where the two ESUs are rotated from Fig. 11a by $\pm\pi/6$. The Raman response is independent of γ , and since one unit moves by $+\delta\varphi$ while the other moves by $-\delta\varphi$, the sum of two expressions (8) gives a total $\delta\chi^{(1)}$ which is strictly zero. This is coherent cancellation. For the HRS response, $\sin 3\gamma = \pm 1$, so that $\sin 3\gamma \delta\varphi = |\delta\varphi|$ for both ESUs. The HRS susceptibilities add, meaning that the total intensity is multiplied by 4. This is perfect constructive coherence.

These opposite coherence effects arise from the general property that $\chi^{(1)}$ is even under inversion, while $\chi^{(2)}$ is odd. For that reason the coherent cancellation of RS for two adjacent ESUs moving symmetrically out-of-phase will always occur. Hence, one should generally expect that coherence negatively affects the RS strength of rigid unit motions, while it is likely to enhance the HRS strength. In the present case, the observed RS BP might amount to just the incoherent contribution, or even less if the coherent cancellation is very effective. For what concerns the HRS strength, $\gamma = \pm\pi/6$ is the most favorable case in the simple model of Fig. 11b. A realistic estimate of the HRS coherent enhancement should take into account that the libration axes of adjacent units need not be parallel. Hence, it seems that only large simulations based on an accurate glass structure will eventually be able to reproduce the experimental result. This would presumably turn out to be an exacting test for the accuracy of the model structure. Very roughly speaking, if N ESUs move in perfect coherence, one would expect a HRS enhancement $\propto N^2$. From Fig. 9, we estimate the HRS BP to be 50 times more intense than the RS one. *If* the latter is fully incoherent, and *if* the HRS and RS coupling strengths are comparable, this could imply a value $N \sim 7$. This very simple estimate makes it clear that this coherence question deserves further investigations.

As a final observation, one should note the slight difference in the maximum position of the RS and HRS BPs in Fig. 9. We find $\omega_{BP}^{HR} \simeq 23 \text{ cm}^{-1}$, while $\omega_{BP}^R \simeq 26 \text{ cm}^{-1}$. The comparison with neutron data shows that the RS BP coincides very well with the *random phase* part⁴⁴ of the reduced vibrational density of states.³⁴ This good agreement presumably results from the incoherent nature of the Raman scattering. The lower position of the HRS BP could thus reflect the coherent enhancement, since HRS would be more effective for coherent packets of larger size which on the average would librate at lower

frequencies.

VII. CONCLUSION

Hyper-Raman scattering has been investigated in v - B_2O_3 . HRS spectra are very different from RS and IR ones, emphasizing the importance of selection rules. Our experimental results motivated an analysis in terms of elementary structural units (ESUs). We assumed a simple structural model involving just one BO_3 triangle and one B_3O_3 boroxol ring. Both belong to the D_{3h} point group. The experiments show that the breathing vibration of boroxol rings (A'_1 mode at 808 cm^{-1}) is silent in IR, and active in RS and HRS, as expected from symmetry considerations. Moreover, its HRS depolarization ratio matches the theoretical value of $2/3$ expected for incoherent non-polar scatterers in the D_{3h} point group. The mode analysis is then applied to the other main features of the HRS spectra of v - B_2O_3 . This allowed identifying the two main polar bands of the IR spectra as the out-of-plane vibrations of triangles and rings around 720 cm^{-1} (A''_2 modes) and as the in-plane vibrations of rings at 1265 cm^{-1} (E' modes). Proceeding by elimination, the BP is then attributed to out-of-plane *librational motions* of rigid boroxol rings *coupled to their relative translations*. The latter are external vibrations of the ESUs that occur naturally at low frequency owing to the relatively weak restoring forces between ESUs. Our conclusion for the boson peak parallels the concept of “rigid unit modes” (RUMs) proposed in Ref^{45,46}. The spectroscopy

reveals that the HRS activity of the BP mainly arises from the librational component (E'' symmetry) of these mixed modes. It has been established several times that the lowest optic-like modes are associated with librations of rigid units in glasses, *e.g.* v - SiO_2 ,^{4,5,47,48} Se ,⁴⁹ and now in v - B_2O_3 (here and in Ref.³⁴). Internal E'' modes are found to be the lowest frequency vibrations in molecular ring systems in the gas state, such as boroxine $H_3B_3O_3$ ¹⁴, or triazine $C_3N_3H_3$ ⁵⁰. Finally, the strong activity of the BP in HRS probably originates from the coherent motion of several adjacent ESUs. A simple example shows how the scattering from two connected ESUs in an out-of-phase E'' motion adds in HRS while it subtracts in RS. Considering the planar isotropy of the Raman tensor of D_{3h} ESUs, symmetry suggests that on the average this effect should enhance the HRS efficiency compared to the RS one. Realistic calculations taking into account the structural disorder of the glass remain to be performed. We do have preliminary HRS results on other glasses showing strong BPs and suggesting similar coherent enhancement. As coherence is presumably related to medium range order, the information provided of HRS could become of considerable value.

The authors express their appreciation to Saint-Gobain Recherche, and in particular to Dr. M.-H. Chopinet and Dr. P. Lambremont, for the availability of their glass preparation facility and for their guidance in obtaining suitable samples. Thanks are also addressed to Dr. A. Matic from Chalmers University for providing samples of lithium borate glasses.

-
- ¹ H. Poulet and J.P. Matthieu, *Vibration Spectra and Symmetry of Crystals*, Gordon and Breach, New York, (1976).
 - ² W.H. Zachariasen, J. Am. Chem. Soc., **54**, 3841 (1932).
 - ³ F.L. Galeener, Solid State Commun. **44**, 1037 (1982).
 - ⁴ U. Buchenau, M. Prager, N. Nücker, A.J. Dianoux, N. Ahmad, and W.A. Phillips, Phys. Rev. B **34**, 5665 (1986).
 - ⁵ B. Hehlen, E. Courtens, R. Vacher, A. Yamanaka, M. Kataoka, and K. Inoue, Phys. Rev. Lett. **84**, 5355 (2000).
 - ⁶ B. Hehlen, E. Courtens, R. Vacher, A. Yamanaka, and K. Inoue, J. Non-Cryst. Solids, **307**, 87, (2002).
 - ⁷ For this reason IR spectroscopy developed into a surface specific probe, see *e.g.* P. Dumas, Surf. Interface Anal. **22**, 561 (2004).
 - ⁸ V.N. Denisov, B.N. Mavrin, and V.B. Podobedov, Phys. Rep. **151**, 1 (1987).
 - ⁹ G.E. Gurr, P.W. Montgomery, C.D. Knutson, and B.T. Gorres, Acta Cryst. **B26**, 906 (1970).
 - ¹⁰ R.L. Mozzi and B.E. Warren, J. Appl. Cryst. **3**, 251 (1970).
 - ¹¹ G.E. Jellison, L.W. Panek, P.J. Bray, G.B. Rouse, J. Chem. Phys. **66**, 802 (1977).
 - ¹² F.L. Galeener, G. Lucovsky, and J.C. Mikkelsen, Jr., Phys. Rev. B. **22**, 3983 (1980).
 - ¹³ P.A.V. Johnson, A.C. Wright, and R.N. Sinclair, J. Non-Cryst. Solids, **50**, 281 (1982).
 - ¹⁴ *E.g.*, J.A. Tossell and P. Lazzeretti, J. Phys. Chem. **94**, 1723 (1990).
 - ¹⁵ J.W. Zwanziger, Solid State NMR **27**, 5 (2005).
 - ¹⁶ P. Umari and A. Pasquarello, Phys. Rev. Lett. **95**, 137401 (2005).
 - ¹⁷ J. Swenson and L. Börjesson, Phys. Rev. Lett. **96**, 199701 (2006).
 - ¹⁸ P. Umari and A. Pasquarello, Phys. Rev. Lett. **96**, 199702 (2006).
 - ¹⁹ A.S. Tenney and J. Wong, J. Chem. Phys. **56**, 5516 (1972).
 - ²⁰ J40-X30SC-106Q from Spectra Physics.
 - ²¹ W.F. Murphy, M. V. Evans, and P. Bender, J. Chem. Phys. **47**, 1836 (1967).
 - ²² LN/CCD 2048-512-EB detector with ST 133A controller from Roper Scientific.
 - ²³ M.A. Ramos, J.A. Moreno, S. Viera, C. Prieto, and J.F. Fernandez, J. Non-Cryst. Solids **221**, 170 (1997).
 - ²⁴ A.C. Hannon, D.I. Grimley, R.A. Hulme, A.C. Wright, and R.N. Sinclair, J. Non-Cryst. Solids, **177**, 299 (1994).
 - ²⁵ A.P. Giddy, M.T. Dove, G.S. Pawley, and V. Heine, Acta Crystallographica, **A49**, 697 (1993).
 - ²⁶ The notation $\chi_{ijk}^{(2)}$ is transformed to contracted indices $\chi_{im}^{(2)}$ with $m = j$ for $j = k$, and $m = 9 - (j + k)$ for $j \neq k$.
 - ²⁷ G. Herzberg, *Molecular Spectra and Molecular Structure, Vol. II, Infrared and Raman Spectra of polyatomic molecules*, Van Norstand, New York (1945).

- ²⁸ S.J. Cyvin, J.E. Rauch, and J.C. Decius, *J. Chem. Phys.* **43**, 4083 (1965).
- ²⁹ R.W. Munn, *J. Chem. Phys.* **114**, 5607 (2001).
- ³⁰ R.W. Munn, M.G. Papadopoulos, and H. Reis, *Polish J. Chem.* **76**, 155 (2002).
- ³¹ R. Bersohn, Yoh-Han Pao, and H.L. Frisch, *J. Chem. Phys.* **45**, 3184 (1966).
- ³² C.F. Windisch, Jr. and W.M. Risen, Jr., *J. Non-Cryst. Solids* **48**, 307 (1982).
- ³³ R.M. Martin and F.L. Galeener, *Phys. Rev. B.* **23**, 3071 (1981).
- ³⁴ G. Simon, B. Hehlen, E. Courtens, E. Longueteau, and R. Vacher, *Phys. Rev. Lett.* **96**, 105502 (2006).
- ³⁵ V.N. Denisov, B.N. Marvin, V.B. Podobedov, Kh. E. Sterin, and B.G. Varshal, *J. Non-Cryst. Solids*, **64**, 195 (1983).
- ³⁶ A.C. Hannon, R.N. Sinclair, and A.C. Wright, *Physica A*, **201**, 375 (1993).
- ³⁷ G. Simon, Doctoral thesis, University Montpellier II, France (2007).
- ³⁸ A. Pasquarello, private communication.
- ³⁹ A.K. Hassan, L.M. Torell, L. Börgesson, and H. Doweidar, *Phys. Rev. B.* **45**, 12797 (1992).
- ⁴⁰ A.V. Baranov, T.S. Perova, V.I. Petrov, J.K. Vij, and O.F. Nielsen, *J. Raman. Spectrosc.* **31**, 819 (2000).
- ⁴¹ D.P. Shelton, *J. Chem. Phys.* **117**, 9374 (2002).
- ⁴² P. Kaatz and D.P. Shelton, *Molecular Physics*, **88**, 683 (1996).
- ⁴³ J.A. Giordmaine, *Phys. Rev.* **138**, A1599 (1965).
- ⁴⁴ D. Engberg, A. Wischniewski, U. Buchenau, L. Börgesson, A.J. Dianoux, A.P. Sokolov, and L.M. Torell, *Phys. Rev. B.* **58**, 9087 (1998).
- ⁴⁵ K. Trachenko, M.T. Dove, K.D. Hammonds, M.J. Harris, and V. Heine, *Phys. Rev. Lett.*, **81**, 3431 (1998).
- ⁴⁶ E.J. Palin, K.O. Trachenko, and M.T. Dove, *J. Phys.: Condens. Matter*, **14**, 4857 (2002).
- ⁴⁷ S.N. Taraskin and S.R. Elliott, *Phys. Rev. B.* **56**, 8605 (1997).
- ⁴⁸ B. Guillot and Y. Guissani, *Phys. Rev. Lett.* **78**, 2401 (1997).
- ⁴⁹ F.J. Bermejo, E. Enciso, A. Criado, J.L. Martinez, and M. Garcia-Hernandez, *Phys. Rev. B.* **49**, 8689 (1994).
- ⁵⁰ C.A. Morrison, B.A. Smart, D.W. Rankin, H.E. Robertson, M. Pfeffer, W. Bodenmiller, R. Ruber, B. Macht, A. Ruoff, and V. Typke, *J. Phys. Chem.*, **101**, 10029 (1997); A. Navarro, J.J. López González, G.J. Kearley, J. Tomkinson, S.F. Parker, D.S. Sivia, *Chemical Physics*, **200**, 395 (1995).